IEEE Photonics Journal
An IEEE Photonics Society Publication

Open Access

Ultralow Power Nonlinear Response in an Si Photonic Crystal Nanocavity

Volume 5, Number 4, August 2013

Yong Zhang
Danping Li
Cheng Zeng
Yu Shi
Zengzhi Huang
Jinzhong Yu
Jinsong Xia

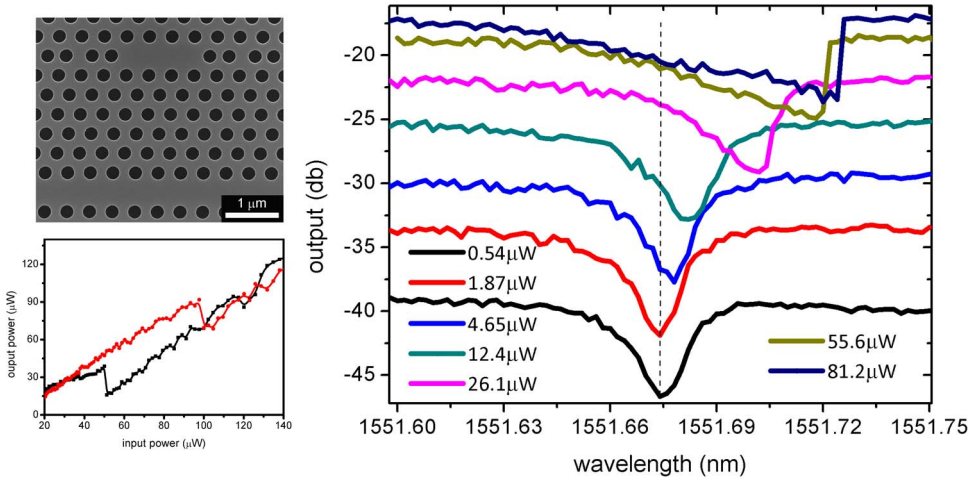

DOI: 10.1109/JPHOT.2013.2273734
1943-0655/$31.00 ©2013 IEEE

Ultralow Power Nonlinear Response in an Si Photonic Crystal Nanocavity

Yong Zhang, Danping Li, Cheng Zeng, Yu Shi, Zengzhi Huang, Jinzhong Yu, and Jinsong Xia

Wuhan National Laboratory for Optoelectronics, School of Optical and Electronic Information, Huazhong University of Science and Technology, Wuhan, Hubei, 430074, China

DOI: 10.1109/JPHOT.2013.2273734

Manuscript received May 27, 2013; revised July 6, 2013; accepted July 9, 2013. Date of current version July 25, 2013. This work was supported in part by the Major State Basic Research Development Program of China under Grants 2013CB632104 and 2010CB923204, by the National Natural Science Foundation of China under Grant 61177049, by the Major State Research Program of China under Grant 2013CB933303, and by the Ph.D. Programs Foundation of the Ministry of Education of China under Grant 20110142120059. Corresponding author: J. Xia (e-mail: jinsongxia@gmail.com).

Abstract: Optical nonlinear response and bistability behavior are observed in a fabricated silicon photonic crystal three defect-long (L3) nanocavity. The L3 cavity, which is coupled with a photonic crystal waveguide, has a quality factor of 60 000. Optical nonlinear response of the L3 cavity is observed at 4.65-μW input power, and the threshold power for optical bistability in the L3 cavity is 26.1 μW, which are the lowest values for silicon L3 cavities. A nonlinear coupled mode model is established to analyze nanocavity characteristics systematically. Numerical simulation results indicate that the ultralow power nonlinearity is due to the high *Q* factor and large thermal resistance of the nanocavity.

Index Terms: Nonlinear optics, integrated optics, photonic crystals, microcavity devices, silicon.

1. Introduction

Due to the rapid development of information society in the last decade, the demand of computation speed and data transmission bandwidth is becoming higher and higher. Photonics is introduced into the data-processing stage to replace traditional electronics, because of its higher operating speed and transmission bandwidth. Furthermore, all-optical processing eliminates power consumption of optical-electrical or electrical-optical signal conversion and can obtain extremely low power consumption. All-optical devices have attracted much attention in the last few years. Optical nonlinearity is one approach to realize optical diode [1]–[3] and all-optical logic gates [4], and bistable devices are versatile foundations for optical signal processing [5]. There are many candidates to achieve bistable devices, including microring resonators [6], periodically structured dielectric waveguides [7] and so on. However, the range of applications of these approaches is limited due to requirement of high input power and low integration density. It's reasonable to fabricate high integrated bistable devices operating at very low input power.

In 2003, physical property and loss mechanism of photonic crystal (PhC) nanocavity was realized clearly [8]. From that, the development of PhC nanocavity has been remarkable, lots of high-*Q*, ultra-high-*Q* and small mode volume PhC nanocavity were fabricated [9]–[11] and applied in various devices, including single-photon sources [12], lasers [13], [14], light emitting diodes [15] and

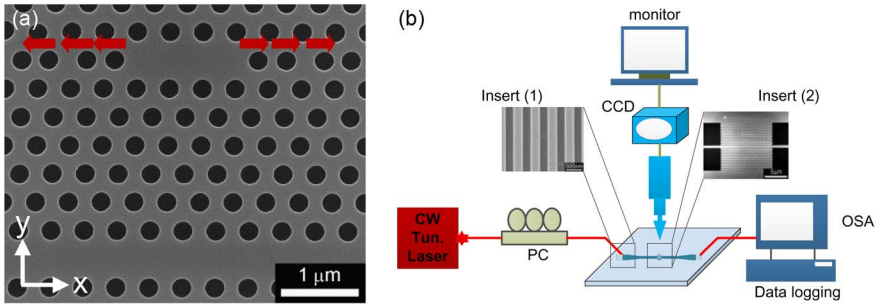

Fig. 1. (a) SEM image of fabricated PhC nanocavity. The three holes adjacent to the cavity are laterally shifted by 0.175a, 0.025a, and 0.175a, respectively. (b) Schematic diagram of measuring apparatus. The inset (1) shows the SEM image of grating couplers, and inset (2) shows the photonic crystal region.

so on. Due to high-Q, small mode volume and strong light-matter interactions of PhC nanocavities, they are also used to enhance nonlinear characteristics [16]–[18].

Bistability at threshold power of $P_{tr} = 1\ \mu$W based on a 2-D GaAs PhC nanocavity was realized by D. Rossi *et al.* in 2007 [19]. M. Notomi and his colleagues obtained sub-femtojoule all-optical switching using an InGaAsP PhC nanocavity in 2010 [20]. However, due to various nonlinear effects in silicon, including thermo-optic effect, Kerr effect and two-photon absorption, it is a large challenge to obtain such low threshold power in silicon nanocavities. Indeed, nonlinear behavior observed at input power 10 μW and low threshold power of $P_{tr} = 40\ \mu$W for optical bistability was achieved using 2-D silicon PhC nanocavity in recent reports [21]–[23]. M. Notomi *et al.* realized $P_{tr} = 1.6\ \mu$W for optical bistability using 1-D silicon nanocavity [24], but P_{tr} of the devices was very sensitive to the characteristic size and length of bridge in the nanocavity. Characteristic size of bridge should be very small (< 100 nm), and length of bridge should be very long. When length of bridge varied from 17 μm to 14.5 μm, P_{tr} increased from 1.6 μW to 63 μW. Such long thin and impending bridge was very difficult to fabricate and very easy to bend to silicon substrate. Silicon 2-D PhC nanocavity may be a better choice. Now it is still a big challenge to realize lower threshold power for optical bistability.

In this paper, we focus on silicon 2-D PhC nanocavity to realize nonlinear response and optical bistability at ultra-low input power. In Section 2, we introduce fabricating processes of our samples and test methods briefly. In Section 3, ultra-low input power nonlinear response and optical bistability in fabricated nanocavity are described. In Section 4, nonlinear coupled mode model is established to analyze the contribution to the nanocavity characteristics of various factors, including Q factor, effective thermal resistance, linear absorption loss and effective free-carrier lifetime. Finally, we conclude our work in Section 5.

2. Fabrication and Experimental Setup

In the experiment, electron beam lithography (Vistec EBPG 5000 plus) and inductively coupled plasma etching were used to define PhC nanocavities on a SOI wafer (220 nm thick silicon on 3000 nm thick silica). A scanning electron microscope (SEM) image of the fabricated sample and a schematic diagram of the measuring apparatus were shown in Fig. 1. L3 cavities with a lattice constant of $a = 420$ nm and a hole radius of $r/a = 0.3$ were fabricated. Optimization of position of the three holes adjacent to the cavity was performed to obtain high Q factor [25], shown in Fig. 1(a). The measuring apparatus was shown in Fig. 1(b), continuous-wave light from a tunable laser was coupled into the waveguide and PhC waveguide by grating couplers and then coupled into the cavity with evanescent-field coupling. The light from through port of devices was coupled out into a fiber and then measured by a spectrometer.

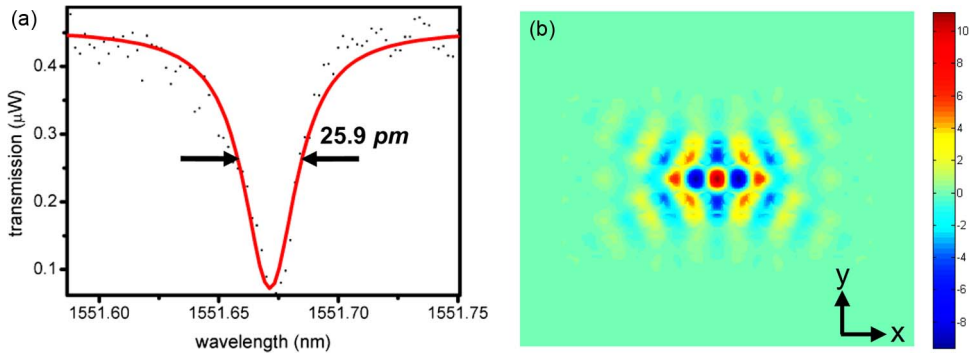

Fig. 2. Resonant mode of L3 cavity. (a) Transmission spectrum in a linear regime. (b) Profile for the Ey field component of resonant fundamental mode.

3. Experimental Results

3.1. Transmission Spectrum in Linear Regime

Fig. 2(a) and (b) showed the transmission spectrum of through port at a very small input power and profile for the Ey field component of resonant fundamental mode, respectively. One resonant dip at 1551.674 nm was observed, the FWHM (full-width-half-maximum) of the resonant dip was 25.9 pm. The measured Q_{total} and T were 60 000 and 18.2% (the transmittance T was defined as the ratio of the transmitting energy in the presence of the cavity near the waveguide to the energy in the absence of the cavity). From the coupled mode theory [26]

$$Q_v = Q_{\text{total}}/\sqrt{T} \tag{1}$$

the estimated vertical Q_v was 141 000 and in-plane Q_{in} was 105 000.

3.2. Transmission Spectra in Nonlinear Regime

Fig. 3(a) showed the transmission spectra of through port at various input powers. The input power was defined as the power coupled into the PhC waveguide, and was calculated from the power at the output port of the tunable laser and coupling efficiency. When input power was increased to 4.65 μW, shown in Fig. 3(b), resonant wavelength of the cavity was red-shifted and transmission waveform became asymmetrical, indicating that nonlinear effects occurred in the nanocavity. The ultra-low input power for observed nonlinear cavity characteristics experimentally, 4.65 μW, was lower than half of previous reports for similar silicon 2-D nanocavities [21]–[23]. As input power increasing, the slope of the transmission waveform on the shorter wavelength side of the dip decreased continually, and the slope on the longer wavelength side of the dip became sharper and sharper. When input power was increased to 26.1 μW, shown in Fig. 3(c), red shift of resonant wavelength reached 28 pm, which was bigger than $\sqrt{3}/2 * FWHM$, where FWHM was the full-width-half-maximum of the resonant dip at very small input power. In addition, a sharp rise was observed on the longer wavelength side of the dip, which was a direct evidence of the bistable behavior of the nanocavity [16], [27]. The threshold power for optical bistability observed experimentally, 26.1 μW, was also lower than previous reports in similar silicon 2-D nanocavities [21]. The threshold power for optical bistability was experimentally obtained by considering the lowest input power for which a sharp rise can be observed and red shift of resonant wavelength reached $\sqrt{3}/2 * FWHM$. Actually, the threshold power obtained from the nonlinear spectra measurement employ here was more accurate than that obtained from the hysteresis curve of the input and output power at a fixed wavelength. The measuring of hysteresis curve was more sensitive to the temperature fluctuation, particularly when the Q factor of the nanocavity was very high.

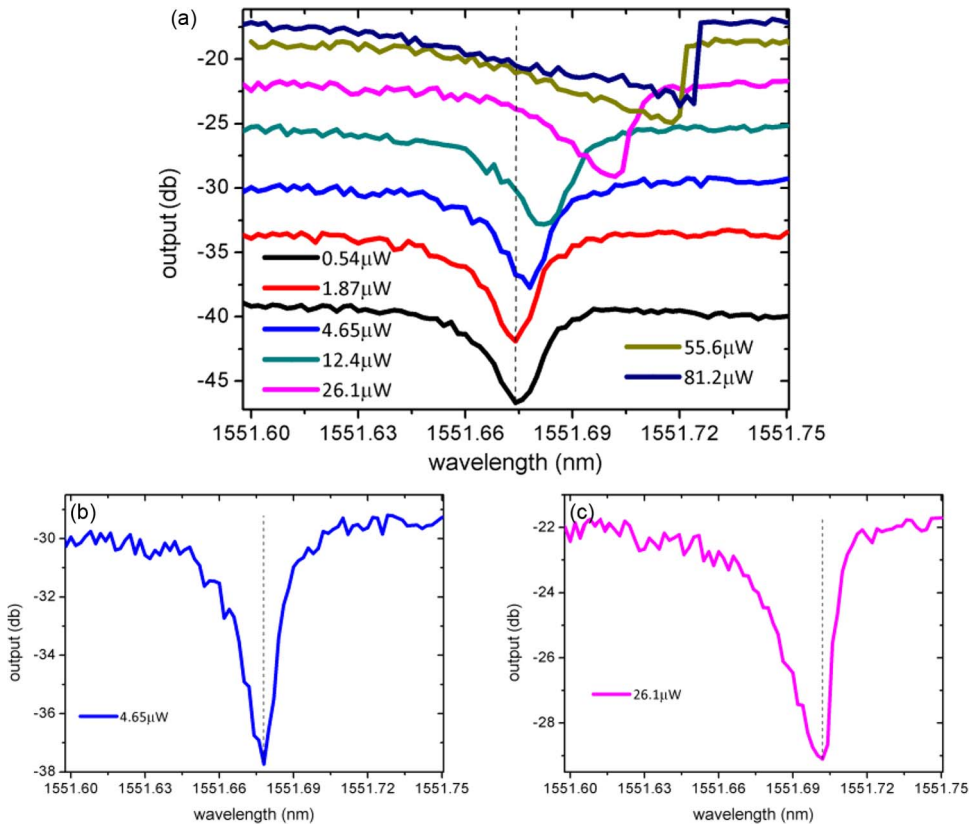

Fig. 3. (a) Transmission spectra in the nonlinear regime at various input powers. (b) Asymmetrical waveform at 4.65 μW. (c) Transmission waveform at 26.1 μW. A sharp rise exists on the longer wavelength side of the dip.

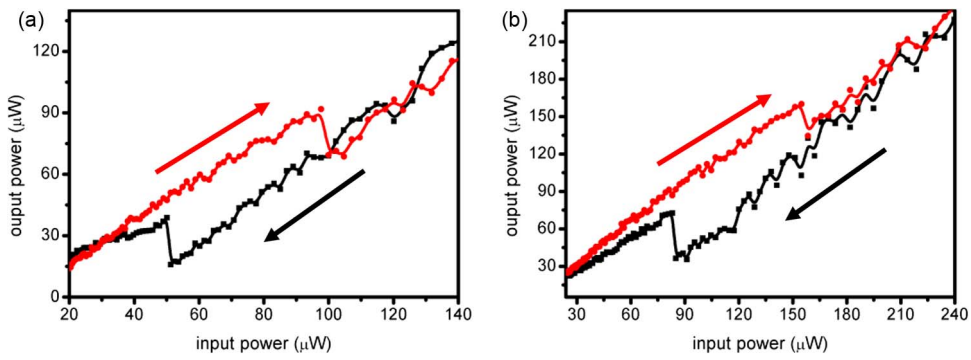

Fig. 4. (a) The hysteresis curve for wavelength detuning $\delta \sim 32$ pm. (b) The hysteresis curve for wavelength detuning $\delta \sim 47$ pm. Red, black lines represented upward and downward sweeps of the power level, respectively. The sweep direction of input powers was also indicated by arrows.

We observed the hysteresis curves in our nanocavity experimentally. We fixed the laser at a wavelength detuned by δ from the resonant wavelength of the cavity, and measured input powers versus output powers for upward and downward sweeps of the power level. As shown in Fig. 4(a), we fixed the input wavelength at 1551.706 nm, which the wavelength detuning δ was 32 pm. Red, black lines represented upward and downward sweeps of the power level, respectively. The clear hysteresis between the OFF and ON branches can be observed. The hysteresis curve for

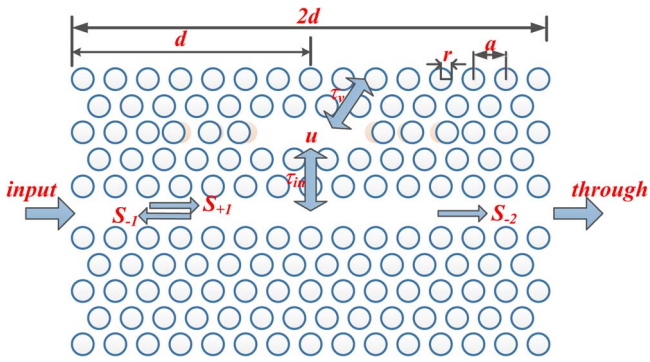

Fig. 5. Coupling in the PhC nanocavity.

wavelength detuning 47 pm was shown in Fig. 4(b). As seen in Fig. 4(b), the switching power increased as δ became bigger.

4. Analysis and Discussion

Due to the high Q factor, long resonant photon lifetimes and small mode volume of PhC cavity here, stored electromagnetic energy density could be extremely large in the cavity. Various nonlinear behaviors may occur in the cavity, including two-photon and free-carrier absorption, thermo-optic effect, plasma dispersion effect and Kerr effect. In addition, linear absorption of "cold nanocavity" (as opposed to radiation in "cold nanocavity") should be also considered in our analysis.

In order to analyze nonlinear behavior in the PhC cavity observed in our experiment, we use nonlinear light propagation equation derived from coupled-mode theory considering nonlinear effects. Linear coupled mode equation is given by [26],

$$\frac{du}{dt} = \left(i\omega_0 - \frac{1}{\tau_{\text{total}}}\right)u + \sqrt{\frac{1}{\tau_{\text{in}}}}e^{-i\beta d}s_{+1} \tag{2}$$

where u is the complex amplitude of light propagating in the PhC nanocavity, which is normalized by letting $|u|^2$ equal to the mode energy, and ω_0 is resonant angular frequency of "cold nanocavity". $1/\tau_{\text{total}}$ and $1/\tau_{\text{in}}$ are the total decay rate and the rate of decay into bus waveguide, respectively. S_{+1} is the complex amplitude of input light in the PhC waveguide, β is the propagation constant in the bus PhC waveguide, shown in Fig. 5.

Due to the crystal symmetry of Si, second-order nonlinear effects can't occur, but third-order nonlinear effects, including two-photon absorption (TPA) and Kerr effect, are expected to be dominant. Since the absorption of light energy through TPA and linear absorption in silicon leads to the generation of free-carriers, free-carrier absorption (FCA) and plasma dispersion effect are also considered in our model. In addition, as the absorbed energy through TPA and linear absorption is finally converted into thermal energy, temperature of Si increases, leading to increases of refractive index n of silicon due to thermo-optic effect. So thermo-optic effect is also taken into account in our model.

Under nonlinear condition, resonant angular frequency of the nanocavity would be

$$\omega' = \omega_0 + \Delta\omega_{\text{thermal}} + \Delta\omega_{\text{plasma}} + \Delta\omega_{\text{kerr}} \tag{3}$$

where $\Delta\omega_{\text{thermal}}$, $\Delta\omega_{\text{plasma}}$, $\Delta\omega_{\text{kerr}}$ are the shifts of resonant angular frequency, due to thermo-optic effect, plasma dispersion effect and Kerr effect, respectively. Detailed nonlinear effect formulas are given by [23]. Total energy decay rates would be,

$$\frac{1}{\tau_{\text{total}}} = \frac{1}{\tau_v} + \frac{1}{\tau_{\text{in}}} + \frac{1}{\tau_{\text{lin}}} + \frac{1}{\tau_{\text{TPA}}} + \frac{1}{\tau_{\text{FCA}}} \tag{4}$$

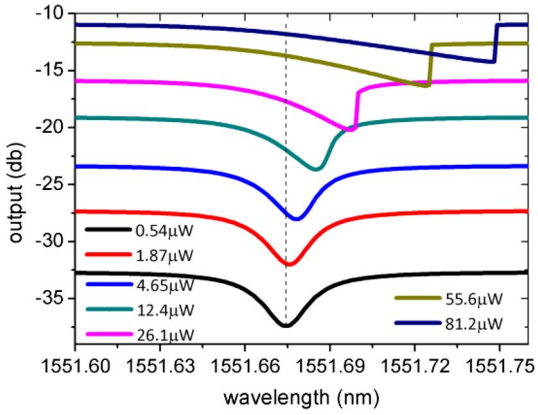

Fig. 6. Calculated transmission spectra of the nanocavity at various input powers.

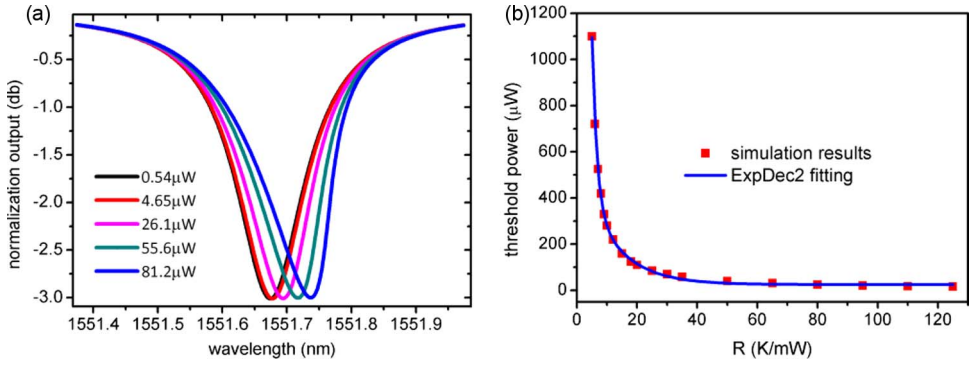

Fig. 7. (a) Calculated transmission spectra of the $Q \sim 10\,000$ nanocavity at various input powers. The axis y represents normalization output, which equals the calculated output power minus input power. (b) Threshold power for optical bistability as a function of thermal resistance of the nanocavity ($Q \approx 60\,000$). Red squares represent simulated results, and the blue line represents the second order exponential decay (ExpDec2) fitting result.

where $1/\tau_{\text{lin}}$, $1/\tau_{\text{TPA}}$, and $1/\tau_{\text{FCA}}$ are decay rates of linear absorption of "cold nanocavity", TPA and FCA, respectively.

With linear coupled mode equation (2) and nonlinear effects equations given by [23], the coupled nonlinear dynamical behavior of our nanocavity system is numerically integrated. Using the physical parameters given by [28], we perform nonlinear coupled mode theory calculations for various input powers used in the experiment and derive the transmission spectra of the nanocavity. The calculation results, shown in Fig. 6, are in good agreement with experiment results presented in Fig. 3. It indicates that nonlinear model derived here can simulate the various nonlinear phenomenon in silicon nanocavities effectively.

In order to analyze the contributions of various factors to the nonlinear effects and bistability in silicon nanocavities, the effects of some parameters, including (i) Q factor of the nanocavity, (ii) effective thermal resistance of the nanocavity, (iii) linear absorption loss of "cold nanocavity", (iv) effective free-carrier lifetime, are investigated by numerical simulations.

Transmission spectra of a nanocavity with a Q factor of 10 000 (FWHM $\sim$155 pm, $Q_v = Q_{\text{in}} = 20\,000$), which is much lower than the Q factor of our fabricated nanocavity, are also calculated using the nonlinear model derived above for comparison, shown in Fig. 7(a). As seen in Fig. 7(a), transmission spectra seem to be almost symmetrical for all the input powers used in our experiment, and there is no sharp rise on the longer wavelength side of the dip. When input power is increased to 81.2 μW, red shift of resonant wavelength is about 63 pm, which is still much lower

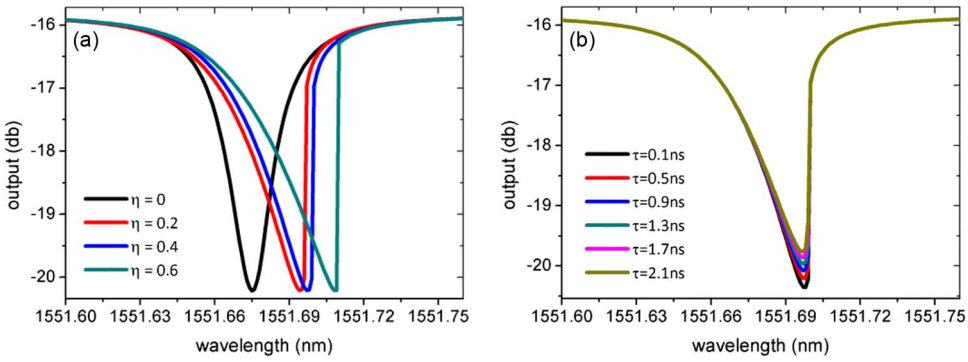

Fig. 8. (a) Calculated transmission spectra of our nanocavity ($Q \sim 60\,000$) with various linear absorption coefficients. (b) Calculated transmission spectra of our nanocavity ($Q \sim 60\,000$) with various free-carrier lifetimes.

than 134 pm ($\sim\sqrt{3}/2 * FWHM$). It indicates that there is no bistability in this low Q nanocavity at this energy level, while optical bistability occurs at input power $\sim$26.1 μW in the high Q ($Q \sim 60\,000$) cavity. The Q factor represents the ability of stored energy in the resonant cavity. Higher Q factor indicates a lower rate of energy loss relative to the stored energy of the resonator; the oscillations die out more slowly. Due to the high Q factor of the cavity and small mode volume, stored electromagnetic energy and energy density could be extremely large, thus optical nonlinearities would be non-negligible. The stored energy density in the low Q factor ($Q \sim 10\,000$) cavity is much lower than the density in the high Q ($Q \sim 60\,000$) cavity, the nonlinear effects in the low Q factor cavity would be much weaker. Therefore, we conclude that observed ultra-low power for optical nonlinearity and bistability in the experiment result from the high Q factor of the nanocavity.

Cavity characteristics are greatly affected by the total refractive index change, which is dominated by thermo-optic effect in the nanocavity. We investigate threshold powers for optical bistability by changing the effective thermal resistance of the nanocavity, which is the ratio of temperature rise to the absorbed energy and determines by mechanical structure of the nanocavity. We take input power, for which a sharp rise can be observed and red shift of resonant wavelength reaches $\sqrt{3}/2 * FWHM$, as threshold power for optical bistability. The results, shown in Fig. 7(b), indicate that as effective thermal resistance increasing, threshold power for optical bistability decreases exponentially. Therefore, if thermal resistance of the nanocavity was much larger, threshold power for optical bistability would be much lower.

In order to achieve larger thermal resistance, the property of thermal confinement in the nanocavity should be much better. As we know, air could be considered a good insulator, and heat almost cannot escape via air, by contrast, silicon is a good heat conductor and heat can pass quickly via silicon. In our silicon 2-D air-bridged PhC nanocavity, the cavity is surrounded by air out of plane, but in the plane, the cavity is connected with silicon slab, which is a path for thermal energy leakage. If the structure of the nanocavity is modified to enhance the confinement of thermal energy, the effective thermal resistance of the nanocavity would increase, leading to an even smaller threshold power for optical nonlinearity and bistability in the nanocavity. Therefore, extremely low threshold power for 1-D nanocavities could be attributed to their good confinement of thermal energy and large thermal resistance.

Transmission spectra of the nanocavity at input power of 26.1 μW are calculated with various linear absorption coefficients, including 0, 0.2, 0.4, and 0.6, shown in Fig. 8(a). Linear absorption coefficient is defined as the ratio of the loss due to linear absorption to the total loss in the "cold nanocavity", $\eta = loss_{\text{lin}}/(loss_{\text{lin}} + loss_{\text{rad}})$. As seen in Fig. 8(a), if we don't consider linear absorption in the model ($\eta = 0$), calculated transmission spectra are almost symmetrical, which are in bad agreement with experiment results presented in Fig. 3. If we take linear absorption η as 0.4, calculated results would be in good agreement with experiment results.

The increase in the density of free-carriers, which are generated through TPA, may lead to plasma dispersion effect. So we investigate the contribution of effective free-carrier lifetime to the cavity characteristics. As shown in Fig. 8(b), transmission spectra of the nanocavity with input power of 26.1 μW and η of 0.4 are calculated with various effective free-carrier lifetimes. We assume free-carrier lifetime as 0.1, 0.5, 0.9, 1.3, 1.7, 2.1 ns here, which is usually 0.5 ns in PhC nanocavity [23]. The results indicate that cavity characteristics are almost identical with lifetime ranging from 0.1 ns to 2.1 ns. In the nanocavity, cavity characteristics are dominated by the total refractive index change due to thermo-optic effect, however, response time of thermo-optic effect is very long relatively and in the order of 1 μs. So free-carrier lifetime ranging from 0.1 ns to 2.1 ns would not influence cavity characteristics.

5. Conclusion

We demonstrated ultra-low power nonlinear response and bistability behavior in silicon 2-D photonic crystal nanocavity experimentally. Nonlinear cavity characteristics were observed at ultra-low power of 4.65 μW, which was lower than half of previous reports, bistability behavior was observed at low power of 26.1 μW, which was also lower than previous reports in similar silicon 2-D PhC nanocavities.

Analysis using the nonlinear coupled mode model presented above indicated that nonlinearity and bistability behavior were mainly attributed to the high *Q* factor and large thermal resistance of the nanocavity here. The optical nonlinearity and bistability were dominated by thermo-optic effect induced by two-photon absorption, free-carrier absorption and linear absorption in silicon nanocavities. Increasing thermal resistance of the nanocavity was an effective method to obtain even lower threshold power for bistability. In addition, we investigated the influence of linear absorption coefficient and free-carrier lifetime to the cavity characteristics.

The ultra-low power nonlinear response and bistability behavior demonstrated here indicate that, high *Q* silicon 2-D PhC nanocavity has great potential for all-optical signal processing.

Acknowledgment

We thank all the engineers in the Center of Micro-Fabrication and Characterization (CMFC) of WNLO for the support in the experiment.

References

[1] L. Fan, J. Wang, L. T. Varghese, H. Shen, B. Niu, Y. Xuan, A. M. Weiner, and M. Qi, "An all-silicon passive optical diode," *Science*, vol. 335, no. 6067, pp. 447–450, Jan. 2012.
[2] L. Fan, L. T. Varghese, J. Wang, Y. Xuan, A. M. Weiner, and M. Qi, "Silicon optical diode with 40 dB nonreciprocal transmission," *Opt. Lett.*, vol. 38, no. 8, pp. 1259–1261, Apr. 2013.
[3] J. Wang, L. Fan, L. Varghese, H. Shen, Y. Xuan, B. Niu, and M. Qi, "A theoretical model for an optical diode built with nonlinear silicon microrings," *J. Lightw. Technol.*, vol. 31, no. 2, pp. 313–321, Jan. 2013.
[4] J. L. O'Brien, G. J. Pryde, A. G. White, T. C. Ralph, and D. Branning, "Demonstration of an all-optical quantum controlled-NOT gate," *Nature*, vol. 426, no. 6964, pp. 264–267, Nov. 2003.
[5] H. M. Gibbs, *Optical Bistability: Controlling Light With Light*. Amsterdam, The Netherlands: Elsevier, 1985.
[6] V. R. Almeida and M. Lipson, "Optical bistability on a silicon chip," *Opt. Lett.*, vol. 29, no. 20, pp. 2387–2389, Oct. 2004.
[7] A. Grieco, B. Slutsky, D. T. H. Tan, S. Zamek, M. Nezhad, and Y. Fainman, "Optical bistability in a silicon waveguide distributed Bragg reflector Fabry-Pérot resonator," *J. Lightw. Technol.*, vol. 30, no. 14, pp. 2352–2355, Jul. 2012.
[8] Y. Akahane, T. Asano, B. S. Song, and S. Noda, "High-Q photonic nanocavity in a two-dimensional photonic crystal," *Nature*, vol. 425, no. 6961, pp. 944–947, Oct. 2003.
[9] B. S. Song, S. Noda, T. Asano, and Y. Akahane, "Ultra-high-Q photonic double-heterostructure nanocavity," *Nat. Mater.*, vol. 4, no. 3, pp. 207–210, Mar. 2005.
[10] E. Kuramochi, M. Notomi, S. Mitsugi, A. Shinya, T. Tanabe, and T. Watanabe, "Ultrahigh-Q photonic crystal nanocavities realized by the local width modulation of a line defect," *Appl. Phys. Lett.*, vol. 88, no. 4, pp. 041112-1–041112-3, Jan. 2006.
[11] J. D. Ryckman and S. Weiss, "Low mode volume slotted photonic crystal single nanobeam cavity," *Appl. Phys. Lett.*, vol. 1017, pp. 071104-1–071104-4, Aug. 2012.
[12] A. Schwagmann, S. Kalliakos, D. J. P. Ellis, I. Farrer, J. P. Griffiths, G. A. C. Jones, D. A. Ritchie, and A. J. Shields, "In-plane single-photon emission from a L3 cavity coupled to a photonic crystal waveguide," *Opt. Exp.*, vol. 20, no. 27, pp. 28 614–28 624, Dec. 2012.

[13] W. Zhou and Z. Ma, "Breakthroughs in Photonics 2012: Breakthroughs in nanomembranes and nanomembrane lasers," *IEEE Photon. J.*, vol. 5, no. 2, p. 0700707, Apr. 2013.
[14] J. D. Sulkin and K. D. Choquette, "Hybrid integration of photonic crystal membrane lasers via postprocess bonding," *IEEE Photon. J.*, vol. 3, no. 3, pp. 375–380, Jun. 2011.
[15] J. Xia, Y. Ikegami, Y. Shiraki, N. Usami, and Y. Nakata, "Strong resonant luminescence from Ge quantum dots in photonic crystal microcavity at room temperature," *Appl. Phys. Lett.*, vol. 89, no. 20, pp. 201102-1–201102-3, Nov. 2006.
[16] J. Bravo-Abad, A. Rodriguez, P. Bermel, S. G. Johnson, J. D. Joannopoulos, and M. Soljacic, "Enhanced nonlinear optics in photonic-crystal microcavities," *Opt. Exp.*, vol. 15, no. 24, pp. 16 161–16 176, Nov. 2007.
[17] J. D. Ryckman and S. M. Weiss, "Localized field enhancements in guided and defect modes of a periodic slot waveguide," *IEEE Photon. J.*, vol. 3, no. 6, pp. 986–995, Dec. 2011.
[18] S. Makino, Y. Ishizaka, K. Saitoh, and M. Koshiba, "Slow-light-enhanced nonlinear characteristics in slot waveguides composed of photonic crystal nanobeam cavities," *IEEE Photon. J.*, vol. 5, no. 2, p. 2 700 309, Apr. 2013.
[19] E. Weidner, S. Combrie, A. de Rossi, N. V. Q. Tran, and S. Cassette, "Nonlinear and bistable behavior of an ultra-high-Q GaAs photonic crystal nanocavity," *Appl. Phys. Lett.*, vol. 90, no. 10, pp. 101118-1–101118-3, Mar. 2007.
[20] K. Nozaki, T. Tanabe, A. Shinya, S. Matsuo, T. Sato, H. Taniyama, and M. Notomi, "Sub-femtojoule all-optical switching using a photonic-crystal nanocavity," *Nat. Photon.*, vol. 4, no. 7, pp. 477–483, Jul. 2010.
[21] M. Notomi, A. Shinya, S. Mitsugi, G. Kira, E. Kuramochi, and T. Tanabe, "Optical bistable switching action of Si high-Q photonic-crystal nanocavities," *Opt. Exp.*, vol. 13, no. 7, pp. 2678–2687, Apr. 2005.
[22] T. Uesugi, B. S. Song, T. Asano, and S. Noda, "Investigation of optical nonlinearities in an ultra-high-Q Si nanocavity in a two-dimensional photonic crystal slab," *Opt. Exp.*, vol. 14, no. 1, pp. 377–386, Jan. 2006.
[23] P. E. Barclay, K. Srinivasan, and O. Painter, "Nonlinear response of silicon photonic crystal microresonators excited via an integrated waveguide and fiber taper," *Opt. Exp.*, vol. 13, no. 3, pp. 801–820, Feb. 2005.
[24] L.-D. Haret, T. Tanabe, E. Kuramochi, and M. Notomi, "Extremely low power optical bistability in silicon demonstrated using 1D photonic crystal nanocavity," *Opt. Exp.*, vol. 17, no. 23, pp. 21 108–21 117, Nov. 2009.
[25] Y. Akahane, T. Asano, B.-S. Song, and S. Noda, "Fine-tuned high-Q photonic-crystal nanocavity," *Opt. Exp.*, vol. 13, no. 4, pp. 1202–1214, Feb. 2005.
[26] L. C. Andreani, P. Andrich, M. Galli, D. Gerace, G. Guizzetti, R. Lo Savio, S. L. Portalupi, L. O. Faolain, C. Reardon, K. Welna, and T. F. Krauss, "Nonlinear optics in silicon photonic crystal cavities," in *Proc. 13th ICTON*, 2011, pp. 1–4.
[27] C. Manolatou, M. Khan, S. Fan, P. R. Villeneuve, H. Haus, and J. Joannopoulos, "Coupling of modes analysis of resonant channel add-drop filters," *IEEE J. Quantum Electron.*, vol. 35, no. 9, pp. 1322–1331, Sep. 1999.
[28] X. Yang and C. W. Wong, "Coupled-mode theory for stimulated Raman scattering in high-Q/Vm silicon photonic band gap defect cavity lasers," *Opt. Exp.*, vol. 15, no. 8, pp. 4763–4780, Apr. 2007.